Singularities of the equations of fluid motion

K. R. Sreenivasan and C. Meneveau
Mason Laboratory, Yale University, New Haven, Connecticut 06520
(Received 8 April 1988)

We explore some implications of the observed multifractal nature of the turbulent energy-dissipation field and of velocity derivatives of increasing order on the near-singularities of the Navier-Stokes equations and the singularities of Euler equations. Although these singularities occur on fractal sets of dimension close to (and only marginally less than) 3, it is shown that most of the energy dissipation is concentrated on a subset of fractal dimension about 2.87 and volume zero. Similar statements can be made with respect to velocity derivatives. In particular, it is shown that the higher the order of the velocity derivative, the less space filling the corresponding singularities become.

I. INTRODUCTION

The subject of singularities of the equations of fluid motion (that is, the Navier-Stokes and Euler equations) has been studied along differing lines of research.[1-7] Mandelbrot[2] conjectured that the set of singularities of the Euler equation is not of the standard Euclidean type but a fractal; he also conjectured that the singularities of the Navier-Stokes equations are essentially those of the Euler equations smoothed by viscosity. The importance of singularities of the equations of fluid motion stems from the realization[8] that a typical procedure for solving the equations of mathematical physics is to set up a list of all characteristic singularities, in the hope that they can be used in appropriate combinations to obtain physical insight about, and solutions to, particular problems. Another reason for this interest is the possibility that they are one of the sources of turbulence in high-Reynolds-number flows.

Some specific results have been obtained by Scheffer[3] regarding the singularities of the Navier-Stokes equations (finite viscosity). In effect, his work shows that the Hausdorff dimension of the set of such singularities is less than two in space time. Caffarelli *et al.*[4] present an even stronger result for certain weak solutions of the Navier-Stokes equations. Even if the Hausdorff dimension of the singularities of the Navier-Stokes equations is no smaller than Scheffer's estimates, it is clear that their intersections by subspaces (that is, by one-dimensional spatial intersections or cuts in time at one point in space) will be empty. Thus, the experimental complement of these mathematical results cannot be explored satisfactorily. On the other hand, one can readily examine how the singularities of the Euler equations manifest themselves in the presence of small amounts of viscosity. This work discusses some results in that direction, which follow logically from our experiments reported earlier[9] on the multifractal nature of the turbulent energy-dissipation rate. We also present new results concerning the multifractal nature of turbulent velocity derivatives up to order four.

We are discussing here spatial regions of a turbulent flow field governed by the Navier-Stokes equations; the boundaries are assumed to be far enough away that they do not control the dynamics of the flow (unlike, for example, in the wall region of the turbulent boundary layer). The only intrinsic scale for the problem is then the Kolmogorov scale η, defined as $(\nu^3/\langle\varepsilon\rangle)^{1/4}$, where ν is the kinematic viscosity of the fluid and ε is the rate of energy dissipation per unit volume given by $(\nu/2)[(\partial u_i/\partial x_j)(\partial u_j/\partial x_i)]^2$, u_i and x_i being the velocity and spatial coordinate vectors, respectively. The quantities of interest here are ε itself, and the velocity gradients of various orders.

Figure 1 shows a linear one-dimensional section of one component of ε, namely $(du_1/dx_1)^2$, obtained via Taylor's hypothesis in the atmospheric boundary layer at a height of several meters above the ground. (Here, u_1 is the velocity component in the mean wind direction x_1.) From this representative component[10] it is clear that ε is highly intermittent, with large magnitudes concentrated in rather small regions. Since the energy dissipation is merely the small-scale manifestation of the energy flux cascading down the inertial range, the tendency of the energy flux to concentrate in small regions can be thought of as related to the near-singular solutions of the Navier-Stokes equations. Similarly, quantities such as $|du^n/dx^n|$, $n > 1$, display regions of large activity interspersed between those of relative quiet, and can be thought of as representing the near-singular characteristics of the governing equations. We are interested in elaborating on these features.

Let ε_r be the energy dissipation rate ε over a box of size r. Typically, ε_r obeys local scaling of the type

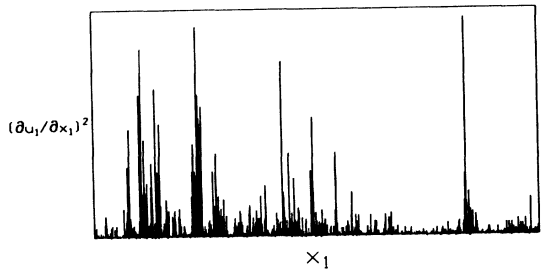

FIG. 1. One-dimensional section through the field of dissipation of turbulent kinetic energy ε in the atmospheric surface layer (for experimental details see Ref. 9).

$$\varepsilon_r \sim \varepsilon_L (r/L)^{\alpha-1} \tag{1}$$

Here, ε_L is the average of ε over boxes of size L—some "large-eddy" scale invoked entirely for the convenience of normalizing r. The result (1) follows from very general considerations based on the invariance of the solutions of the Navier-Stokes equations under simple transformations (see, for example, Refs. 9 and 11). The total dissipation E_r in a d-dimensional box of size r (volume r^d) will therefore obey the local scaling

$$E_r \sim E_L (r/L)^{\alpha-1+d} . \tag{2}$$

Because of the large variability in ε_r or E_r for small r, it is to be expected that α is a function of the spatial coordinate x, say, of the center of the box. Let $N_r(\alpha)$ be the number of boxes of size r which α takes on a certain value between α and $\alpha+d\alpha$. Typically for multifractals,[9,11,12] one has that $N_r(\alpha)$ follows a power law with r:

$$N_r(\alpha) \sim (r/L)^{-f(\alpha)} . \tag{3}$$

where $f(\alpha)$ is usually interpreted as the fractal dimension of iso-α sets. The entire dissipation field can be thought of as being constituted of a superposition of interwoven iso-α sets with α varying between an $\alpha_{\min}$ and an $\alpha_{\max}$, f being a function of α. The curve of f versus α will then describe the multifractal distribution of the dissipation field.

It is seen from Eq. (1) that as $r \to 0$, $\varepsilon_r \to \infty$ for all $\alpha < 1$, which thus represents the singularities related to the dissipation field in the limit of zero viscosity (infinite Reynolds number). Conversely, dissipation occurring in regions with $\alpha > 1$ is regular in that it not only remains bounded but also tends to zero as the averaging volume shrinks to zero. For the Navier-Stokes equations, it is clear that the smallest scale of dynamical importance is η, and fluctuations on smaller scales are smoothed out by viscosity; the singular behavior in a strict mathematical sense does not therefore obtain. Even so, for $\alpha < 1$, large values of $\varepsilon_\eta \sim \varepsilon_L (\eta/L)^{\alpha-1}$ exist, with the largest ε_η being given by $\varepsilon_L (\eta/L)^{\alpha_{\min}-1}$. The picture, then, is that the near-singularities observed in the finite-viscosity case are the singularities smoothed out by viscosity. One of the tacit implications here is that the viscosity effects are essentially benign. We shall return to this statement in Sec. IV.

II. EXPERIMENTAL RESULTS

A. The dissipation field

We have obtained in Ref. 9 the $f(\alpha)$ curve for one-dimensional sections of the energy-dissipation field in a number of turbulent flows. Details of measurement as well as assessment of their accuracy can be found in that reference, where it has also been shown that the $f(\alpha)$ curve is universal for a variety of fully turbulent flows. That is, the precise value of the Reynolds number and the details of the flow are irrelevant as long as turbulence is fully developed. Figure 2 shows the mean curve drawn through the experimental $f(\alpha)$ curve.

Before proceeding further, we must remark on the validity as well as the limitation of the method of one-dimensional intersections used to obtain the $f(\alpha)$ curve. The general expectation is that the linear intersections of the dissipation field in three dimensions posses fractal dimensions which are 2 less than that of the dissipation field itself. Such additive rules are expected to hold for isotropic fractals, which are such that the resulting dimension is independent of the orientation of the intersecting plane or line (see Ref. 8, and references cited on p. 366). It is generally believed[15,16] that the dissipation structures in turbulence are spatially isotropic in a statistical sense, so that any one-dimensional spatial cut can be expected to be independent of the multifractal itself. By comparing results from one- and two-dimensional sections, we have previously shown that the additive law holds for scalar interfaces,[17] as well as for the multifractal description of the scalar dissipation field.[18]

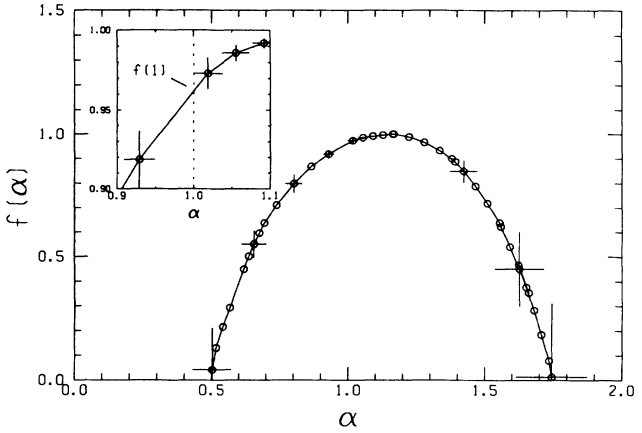

FIG. 2. Universal f vs α curve of one-dimensional sections of ε in fully developed turbulence and experimental variability (Ref. 9). This curve was obtained by first measuring the generalized dimensions (Refs. 13 and 14) D_q for 13 values of q between -6 and 6. By linear interpolation of the D_q curve, a total of 36 points was generated, which was then used to obtain α and $f(\alpha)$ by center differencing. The inset shows the magnification of the curve in the neighborhood of $\alpha = 1$.

The essential conclusion for three dimensions is that $f^*(\alpha) = f(\alpha) + 2$ for $2 \le f^*(\alpha) \le 3$, where the superscript asterisk denotes quantities relevant to three-dimensional space. In Fig. 3, we schematically compare $f(\alpha)$ with $f^*(\alpha)$. The top part of the curve in the range $2 \le f^*(\alpha) \le 3$ is identical in both cases, whereas the part $f^*(\alpha) < 2$ is largely inaccessible in line-intersection methods because such intersections will in general be null sets. It is then clear that $\alpha^*_{\min} \le \alpha_{\min}$ and that $\alpha^*_{\max} \ge \alpha_{\max}$. Noting that the bottom part of the curve should intersect the line $f^*(\alpha) = 0$ perpendicularly, the differences in the maximum and minimum values of α in the two cases will be relatively small. The fact that we can determine by intersection methods only those singularities whose fractal dimension exceeds 2 turns out to be no serious restriction because, as we shall see, the important case corresponds to $f^*(\alpha) > 2$.

If S is the union of all (disjoint) regions corresponding to $\alpha < 1$, then S can be regarded as the support of the singularities of the dissipation field—singularities mean-

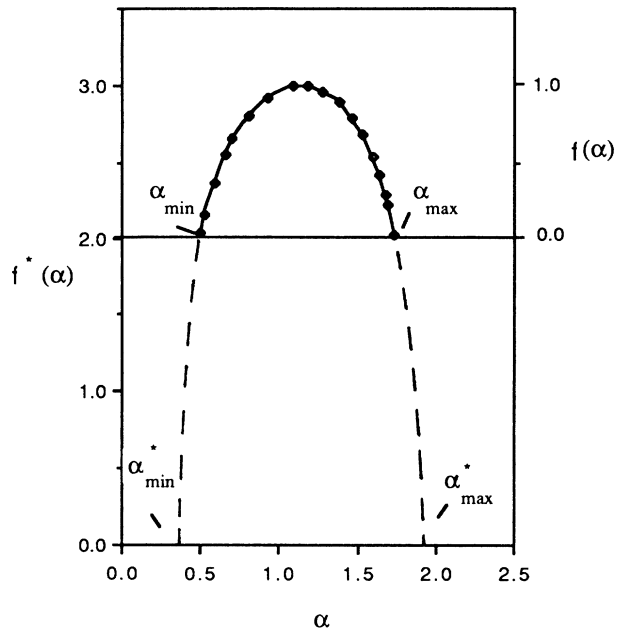

FIG. 3. Schematic of the $f(\alpha)$ curves in three dimensions compared with that obtained by line intersections.

ing that $\varepsilon_r \to \infty$ in the double limit $r \to 0$ and $\nu \to 0$. The number of boxes N_η of size η needed to cover S is given by

$$N_\eta(S) = \int_{\alpha<1} N_\eta(\alpha) d\alpha \sim \int_{\alpha<1} (\eta/L)^{-f(\alpha)} d\alpha \ . \quad (4)$$

For small values of η/L (large Reynolds number), the integral is dominated by the term for which $f(\alpha)$ is maximum in the range $\alpha < 1$, and since the f versus α curve increases monotonically in that range, the dominant term is clearly $(\eta/L)^{-f(1)}$. Therefore

$$N_\eta(S) \sim (\eta/L)^{-f(1)} \ , \quad (5)$$

and we can conclude that the fractal dimension of the set of singularities of the dissipation field is $f(1)$. From Fig. 2, $f(1)$ is about 0.96.

As we shall see later, the important point is that $f(1) < 1$, not its precise numerical value. To show that $f(1)$ is definitely less than unity, we first comment on the experimental accuracy and then note other reasons for expecting this result. Figure 2 shows that the error bars on the $f(\alpha)$ curve are of different magnitudes at different values of α and are quite small near $\alpha = 1$. This can be seen better by returning to the generalized dimensions[13,14] D_q from which the $f(\alpha)$ curve was computed in Ref. 9. The error bar for $q = 0$ is essentially zero, consistent with the expectation that $D_0 = 1$ (that is, there is some dissipation everywhere). The error bar is finite but small in the neighborhood of $q = 0$, as the inset to Fig. 2 shows. It is clear that the conclusion that $f(1) < 1$ holds outside of experimental uncertainties.

Alternatively, expanding the $f(\alpha)$ curve around the maximum of f, which occurs at $\alpha = \alpha^* > 1$ (see Fig. 2), we have

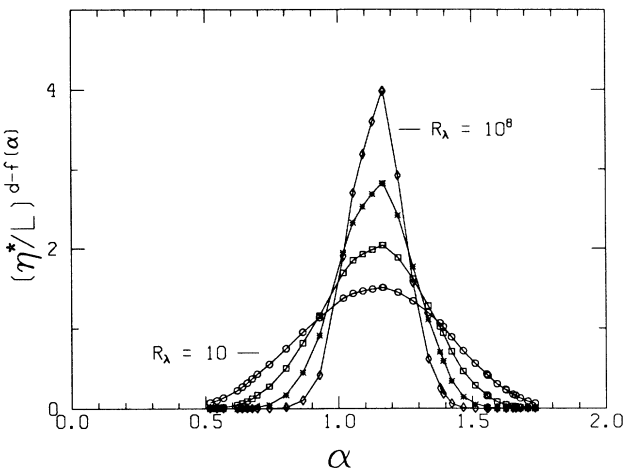

FIG. 4. Variation of $(\eta^*/L)^{d-f(\alpha)}$ (fractional volume occupied by sets with a specific value of α) as functions of α and R_λ (Reynolds number based on the Taylor microscale). In this figure as well as Fig. 5, the areas under the different curves are normalized to unity.

$$f(\alpha) = f(\alpha^*) + (df/d\alpha)_{\alpha=\alpha^*}(\alpha-\alpha^*) + (d^2f/d\alpha^2)_{\alpha=\alpha^*}(\alpha-\alpha^*)^2/2 + \cdots \ .$$

Since $(df/d\alpha)_{\alpha=\alpha^*} = 0$, and $(d^2f/d\alpha^2)_{\alpha=\alpha^*} < 0$ by the concavity of the $f(\alpha)$ curve—see, for example, Ref. 12, p. 1142)—we have the result that $f(\alpha)$ must be less than 1 in the vicinity of α^*. As an aside, we note that the concavity condition on the $f(\alpha)$ curve is related to the thermodynamic stability of the pseudostatistical mechanical system that generates the $f(\alpha)$ curve.

Finally, the physical result that the turbulent energy dissipation rate in a finite volume must be finite also constrains $f(1)$ to be less than unity. The set corresponding to some α slightly less than unity has a dissipation rate given by $\varepsilon \sim r^{\alpha-1}$, which tends to infinity as $r \to 0$. If such a set were space filling, the energy dissipation would

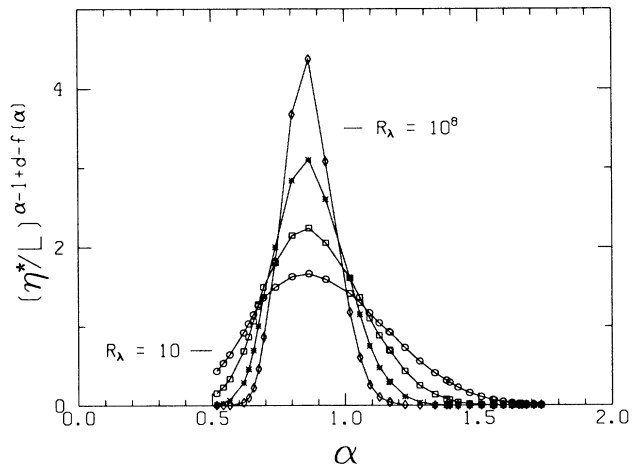

FIG. 5. Variation of $(\eta^*/L)^{\alpha-1+d-f(\alpha)}$ (the dissipation contained in regions with a specific value of α), as functions of α and R_λ.

be infinite. This unphysical result can be avoided only by stipulating that the value of f corresponding to this α must be less than unity. Since this argument can be extended to all α's approaching unity from below, we conclude that $f(1)$ must be less than 1.

From the previous discussion on the additive rules for intersection,[8] we conclude that the fractal dimension of the set of singularities of ε is definitely (though only marginally) less than 3; its approximate value is about 2.96.

Some secondary quantities, related to how fast in Reynolds number the Euler limit is achieved, can be determined from this analysis. First, using Eq. (4), we see that the fraction of volume occupied by the singular set S is

$$V(S)\sim\int_{\alpha<1}(\eta/L)^{d-f(\alpha)}d\alpha\ . \tag{6}$$

In writing Eq. (6) it has been assumed that the preexponential factor in (3) is a constant. At present, there is no experimental information on this point, and we have invoked it merely for simplicity.

Similarly, the fraction of the total dissipation within the singular regions is given by integrating (1) for all $\alpha<1$, that is,

$$E(S)\sim\int_{\alpha<1}(\eta/L)^{\alpha-1+d-f(\alpha)}d\alpha\ . \tag{7}$$

To determine the variation of $V(S)$ and $E(S)$ with respect to Reynolds number, one can approximate the local Kolmogorov scale η in Eqs. (6) and (7) by its representative average η^* given by $(\nu^3/\langle\varepsilon\rangle)^{1/4}$, and use the relation[9] $(\eta^*/L)\sim R_\lambda^{-3/2}$, R_λ being the microscale Reynolds number. The effect of this approximation, made here for convenience, will be shown later in this section to be negligible.

In Figs. 4 and 5 we have plotted the quantities $(\eta^*/L)^{d-f(\alpha)}$, and $(\eta^*/L)^{\alpha-1+d-f(\alpha)}$ as functions of α for four different Reynolds numbers R_λ of 10, 10^2, 10^4, and 10^8. In both figures, the areas are normalized to be the same for all four Reynolds numbers. The fractional area for $\alpha<1$ in each of the four curves in Fig. 4 gives the quantity expressed in Eq. (6) above—which, as remarked already, is the volume occupied by the near-singular regions of the dissipation field. Similar fractional areas for $\alpha<1$ in Fig. 5 represent the quantity (7), which is the amount of dissipation concentrated in regions of near-singularity.

In Fig. 6 variations of $V(S)$ and $E(S)$ with R_λ are shown by a solid line; the dashed lines will be explained below. As expected on intuitive grounds, the volume of the near-singular regions $V(S)$ goes down to zero as $R_\lambda\to\infty$, while the entire dissipation tends to concentrate in these regions of diminishing volume.

As remarked already, one can redo these calculations by taking the local value of η instead of η^*. Noting that $\eta/\eta^*\sim(\langle\varepsilon\rangle/\varepsilon)^{1/4}$, and that $\varepsilon\sim\langle\varepsilon\rangle(\eta/L)^{\alpha-1}$, we have the result that

$$(\eta/L)\sim(\eta^*/L)^{4/(\alpha+3)}\ . \tag{8}$$

Thus replacing η/L in Eqs. (6) and (7) by the right-hand side of Eq. (8), we get the dashed curves in Fig. 6 instead of the continuous curve. There is very little difference between them.

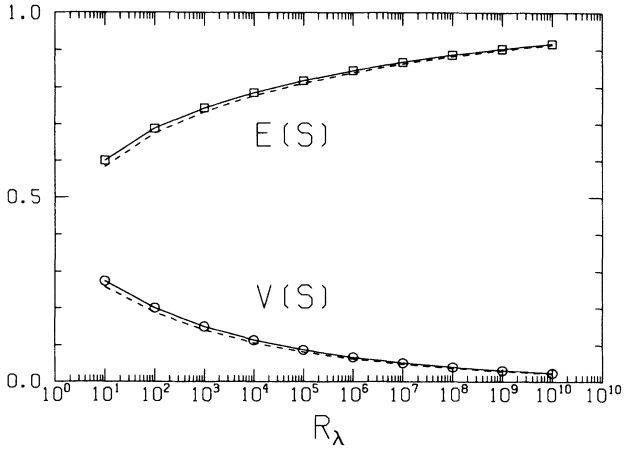

FIG. 6. Fraction of volume occupied by the near-singular regions of the dissipation field $V(S)$ as function of R_λ (lower curve), and fraction of total dissipation occurring in the near-singular regions $E(S)$ as function of R_λ (upper curve). If the effects of spatial fluctuations in η are included, one obtains the dashed lines (see text).

The results of Figs. 4–6 are easy to understand. Small α implies large intensity of dissipation [see Eq. (1)], but such sets occupy small volume because f is close to zero [see Fig. 2 and Eq. (6)]. On the other hand, sets corresponding to larger α occupy larger volumes but possess low-intensity dissipation; the largest α sets have low dissipation as well as occupy small volumes, and are therefore unimportant. It is clear that the largest contribution to the total amount of dissipation occurs for some intermediate α minimizing the exponent in Eq. (7). This yields the condition $f'=\partial f/\partial\alpha=1$. Noting that $f'=1$ occurs at $f=\alpha$ [this being a property of all $f(\alpha)$ curves], it is seen from Fig. 2 that the integrand of (7) must peak at $\alpha=0.87$. Figure 5 is consistent with this expectation.

Three further points need amplification. First, in the limit $R_\lambda\to\infty$, the peak in the figure can be expected to become increasingly sharper, approaching a delta function centered around $\alpha=0.87$. It then follows that most of the dissipation is concentrated (in one-dimensional sections) on a fractal set of dimension 0.87 and volume zero. We conclude that the fractal dimension of this set is about 2.87 in three-dimensional space. Second, from the Legendre transform between the pairs of variables (f,α) and (D_q,q), it is clear that the condition that $f=\alpha$ and $df/d\alpha=1$ corresponds to the set whose dimension is the information dimension D_1. Thus, a statement that all the dissipation is concentrated near $f=\alpha$ is equivalent to saying that it occurs on a set of dimension D_1. The specific meaning[20] of the information dimension is that it represents the amount of information necessary to specify the state of the system to within the resolution employed. Equivalently, for canonical systems in statistical mechanics, the distribution of the probability measure on a set of dimension D_1 maximizes the amount of disorder under the constraint of the observed values of internal energy. The interpretation becomes clear if we recognize[21,22] that measuring the $f(\alpha)$ or the D_q curve corresponds to

measuring the thermodynamic quantities of the pseudo-statistical mechanical system being analyzed. The implication therefore is that the turbulent energy dissipation is distributed in such a way that disorder is maximized subject to the constraints of the observed distribution of α. Finally, we note that the modeling of the dissipation field by singularities of strength $\alpha=0.87$ lying on a set of fractal dimension 2.87 yields the β model[23] for fractally homogeneous turbulence.

B. Velocity derivatives

Here, we wish to examine the singularities of the spatial derivatives of the velocity field $u(x)$. Mandelbrot[2] conjectured that the singularities of velocity derivatives of increasing order lie on sets which become increasingly less space filling. To examine this, we have analyzed experimentally the one-dimensional sections of $|\partial^n u_1/\partial x_1^n|$, the absolute value of the nth-order "streamwise" derivative of the streamwise turbulent velocity. For convenience of representation, we subsequently replace u_1 by u and x_1 by x. A few words are in order on the first derivative $|\partial u/\partial x|$. Since it is proportional to $\varepsilon_\eta^{1/2}$, it can be shown (for details see Appendix A) that the f versus α curves of ε and $|\partial u/\partial x|$ are related for one-dimensional sections by

$$\alpha_u=(\alpha+D_{1/2})/2\ , \tag{9}$$

$$f_u(\alpha_u)=f(2\alpha_u-D_{1/2})\ , \tag{10}$$

where the subscript u refers to $|\partial u/\partial x|$, and the unsubscripted quantities refer to ε. Figure 7 shows a comparison between the experimental f versus α curve obtained directly for $|\partial u/\partial x|$ (dashed line), and Eqs. (9) and (10) applied to the average experimental f versus α curve of ε (continuous line). The agreement is good within experimental scatter. Thus the first derivative of the velocity is a multifractal, and its f versus α curve can be related to that of ε. Higher-order derivatives, however, contain additional information. We verified that one-dimensional sections through $|\partial^n u/\partial x^n|$ can be treated as multifractal measures and obtained their f versus α curves for different values of n up to 4. Details of the experimental procedure, as well as an assessment of the accuracy in evaluating the derivatives, are given in Appendix B.

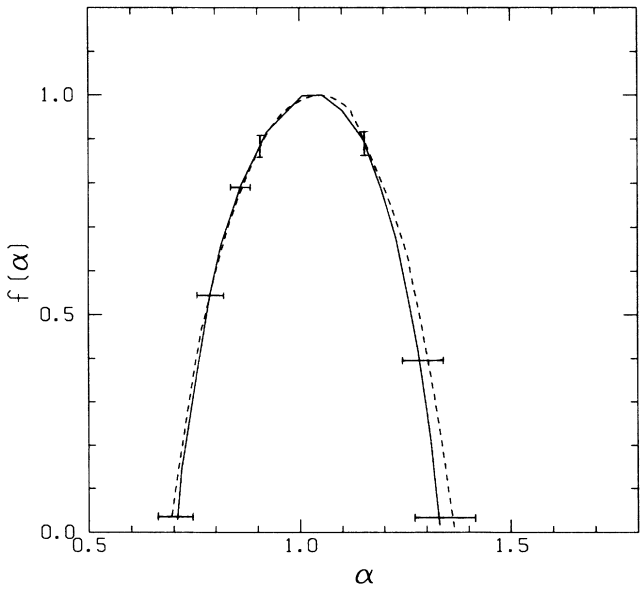

FIG. 7. Comparison between measured f vs α curve for $|\partial u/\partial x|$ (dashed line) and transformations [Eqs. (9) and (10)] applied to the f vs α curve of ε in Fig. 2 (continuous line). The error bars show typical experimental variability.

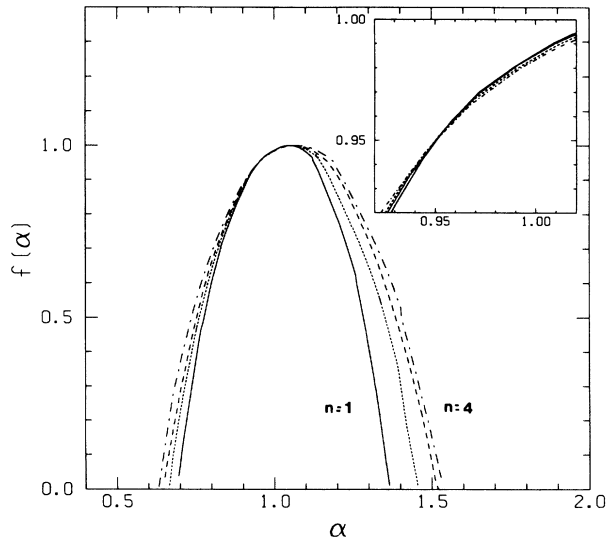

FIG. 8. f vs α curves of velocity derivatives $|\partial^n u/\partial x^n|$ for $n=1$–4. Typical experimental variability is as shown with error bars in Fig. 7.

Figure 8 shows the f versus α curves of $|\partial^n u/\partial x^n|$ for n from 1 to 4. For larger n, $\alpha_{\min}$ decreases (Fig. 9), showing that the strength of the largest singularity increases with the order of the derivative. One may note that the f versus α curve of $|\partial^n u/\partial x^n|$ for $n=0$ (just the absolute value of u) is a single point at $\alpha=1$ and $f(\alpha)=1$; that is, one does not observe any singularlike behavior in u itself. The quantity $\alpha_{\min}$ for $n=0$ is therefore unity and is included in Fig. 9 for completeness.

With respect to the fractal dimension $f(1)=f(\alpha=1)$ of the set supporting the near-singularities of $|\partial^n u/\partial x^n|$, we note that the f versus α curves in Fig. 8 intersect at some intermediate value of α between $\alpha_{\min}$ and $\alpha=1$; as a

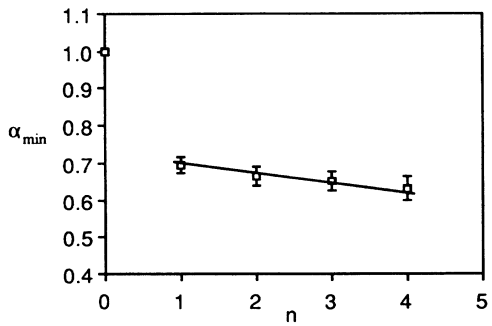

FIG. 9. Variation of minimum scaling exponent $\alpha_{\min}$ (corresponding to the strongest singularities) with the order n of the derivative.

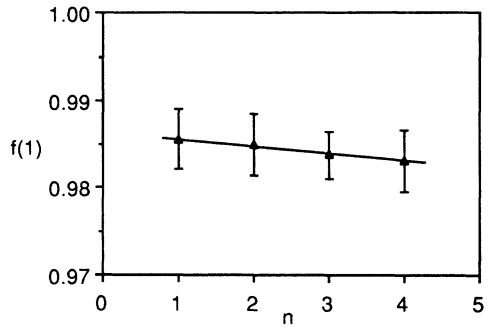

FIG. 10. Variation of the fractal dimension $f(1)$ of the set of near-singularities of $|\partial^n u/\partial x^n|$ with the order n of the derivative.

result, $f(1)$ decreases with increasing n, as made explicit in Fig. 10. The conclusion therefore is that the singularities, observed in the multifractal measures of $|\partial^n u/\partial x^n|$ at least for n up to 4, reside on sets whose fractal dimension is a decreasing function of n, substantiating Mandelbrot's conjecture. Again, it is worth noting that the decrease of $f(1)$ with n is extremely slow and that $f(1)$ is very close to the dimension of the embedding space for the values of n treated here.

III. RESULTS FROM THE p MODEL

It has been shown elsewhere[24] that the multifractal dissipation field can be modeled quite satisfactorily by a two-scale Cantor measure, and we invoke this model (the p model) to provide expressions for f versus α that are easy to manipulate analytically. Briefly, the model describes a low-order approximation to the real cascading process of energy in the inertial range, whose thermodynamic or macroscopic description[21,22] is given by the measured f versus α curve or, equivalently, by the generalized dimensions D_q. Excellent agreement (at this thermodynamic level of description) between the model and the measurements is obtained by assuming that, at each stage of the cascade, half of the newly generated, equal-sized eddies receive a fraction $p_1=0.7$ of the energy flux, while the other half receives the remaining fraction $p_2=0.3$. The q dependence of D_q for one-dimensional sections with the p model is given by

$$D_q=\log_2(p_1^q+p_2^q)/(1-q) , \tag{11}$$

where D_q is defined by

$$\sum(E_r/E_L)^q\sim(r/L)^{(q-1)D_q} \tag{12}$$

and the sum is taken over all boxes of size r.

Using the typical Legendre transformation[12] which relates the pairs (q,D_q) and $[\alpha,f(\alpha)]$, we see that the condition $\alpha<1$ is equivalent in the p model to

$$q>Q=\frac{\log_2[\log_2(2p_2)^{-1}/\log_2(2p_1)]}{\log_2(p_1/p_2)} . \tag{13}$$

Using $p_1=1-p_2=0.7$, we get $Q=0.493$. In addition, $f(1)$ for linear intersections can be written as

$$f(\alpha=1)=q\alpha-(q-1)D_q$$
$$=Q-(Q-1)D_Q=0.969 , \tag{14}$$

which agrees with measurement [see discussion immediately following Eq. (5)].

The value of Q has an interesting interpretation. For $q>Q$, $\langle\varepsilon_\eta^q\rangle$ is determined largely by dissipation occurring on the set S, the singular part of dissipation. For $q<Q$, however, this average is dominated by regions in which the dissipation is regular. Noting that $|\partial u/\partial x|\sim(\varepsilon_\eta/\nu)^{1/2}$, we argue that the global average of the absolute value of the velocity gradient is dominated by the region where energy dissipation is singular, simply because $Q<\frac{1}{2}$.

For the p model it is also clear that $f'=1$ occurs at

$$f=\alpha=-(p_1\log_2 p_1+p_2\log_2 p_2) , \tag{15}$$

which gives 0.88 for $p_1=1-p_2=0.7$, very close to the measured value of 0.87.

The generalization of the p model to three dimensions implies that each one of the 2^3 subeddies receives either a fraction $p_1/4$ or $p_2/4$ of the energy flux received by their predecessor. The $f^*(\alpha)$ curve of such a process would be like Fig. 3, with $\alpha^*_{\min}=\alpha_{\min}$ and $\alpha^*_{\max}=\alpha_{\max}$. In order to include some singularities with $f^*(\alpha)<2$, one can slightly perturb the ratios of energy fluxes around $p_1/4$ and $p_2/4$ for each of the 2^3 new subeddies (these perturbations being subject to the conservation of energy flux), and obtain $f^*(\alpha)$ curves with $\alpha^*_{\min}<\alpha_{\min}$ and $\alpha^*_{\max}>\alpha_{\max}$. The magnitude of such perturbations is expected to be small if the limiting α values of the $f(\alpha)$ and $f^*(\alpha)$ curves do not differ very much.

IV. CONCLUSIONS

We have used the experimental results of Ref. 9 to quantify some aspects of the singularities of the equations of motion. On the basis of the mathematical results of Refs. 3 and 4 on the dimension estimates of the singularities of the Navier-Stokes equations, it is clear that one cannot determine them efficiently by line-intersection methods. It follows that the present results must refer to Euler equations, the fluid viscosity serving the sole function of smoothing out the singularities by setting a suitable cutoff. It is also clear that line-intersection methods are not useful for detecting the extremely rare and intense singularities of the Euler equations, but we have shown that their rareness makes them unimportant, though not uninteresting, in practice. To detect them, one has to search the entire three-dimensional space. It is plausible that such a search can also detect the singularities of the Navier-Stokes equations discussed in Refs. 3 and 4, where the role of viscosity will be dynamic. Efforts in this direction are continuing.

One of our principal results on the singularities of ε is that they occur on a set S of fractal dimension 2.96. It came as a surprise that these singularities are so close to space filling. However, most of the dissipation is concentrated on a proper subset of S of fractal dimension 2.87 (but volume zero). From this result, it is difficult to obtain unambiguously the true geometric nature of the dis-

sipation field. Kuo and Corrsin[25] examined this issue by multiprobe measurements, and concluded that these structures are more likely to be sheetlike than bloblike or tubelike. If this is true, it appears that the dynamic processes leading to fully developed turbulence consists intrinsically of stretching and folding the sheetlike structures in a manner qualitatively similar (in physical space) to what happens in establishing (for example) a strange attractor (in phase space). The essential ingredients required to augment this picture will then be the principal rates of strain, which are analogous to the "Lyapunov exponents" in phase space. Although some information on these quantities is now available,[26] it is not yet clear how it can be incorporated in any quantitative way. Another possibility consists of stretching of vortex filaments, a subject that has been explored using analogies to polymer chains.[27–29]

The present results on the singularities of the velocity derivatives of order $n > 1$ show that they too are concentrated on fractal sets of dimensions close to, but less than, 3. In particular, we have shown that these singularities become increasingly less space filling as the order of the velocity derivative increases.

We believe that these considerations are important in the context of high-Reynolds-number mixing (of momentum, species, heat, etc.).

ACKNOWLEDGMENTS

We thank A. Chhabra and M. Nelkin for some useful discussions and the National Science Foundation and Defense Advanced Research Projects Agency for financial assistance.

APPENDIX A

We address here the relationship between the f versus α curves of ε and $|\partial u/\partial x|$. Recalling that

$$\varepsilon_\eta \sim \nu |\partial u/\partial x|^2 \tag{A1}$$

and defining $|\partial u/\partial x|_r$ as the integral of $|\partial u/\partial x|$ over a box of size r, it is easy to show that

$$|\partial u/\partial x|_r = K_1 \sum E_\eta^{1/2} . \tag{A2}$$

Here K_1 is a constant that depends only on ν and η, E_η is the dissipation contained in regions of size η, and the sum extends over all $(r/\eta)^d$ boxes contained within the box of size r.

As in Eq. (2), if $|\partial u/\partial x|$ is a multifractal, we can write locally that

$$|\partial u/\partial x|_r \sim r^{\alpha_u - 1 + d} , \tag{A3}$$

where α_u is now the strength of singularities of $|\partial u/\partial x|$. Let us rewrite Eq. (A2) as

$$|\partial u/\partial x|_r \sim K_1 E_r^{1/2} \sum (E_\eta/E_r)^{1/2} . \tag{A4}$$

In order to evaluate the sum of $(E_\eta/E_r)^{1/2}$ within the box of size r we have to make use of the definition of the generalized dimensions as stated in Eq. (11). In addition, we can use the self-similar properties of multifractals and write Eq. (11) for $q = \frac{1}{2}$, replacing r by η, and L by r, provided that $\eta \ll r \ll L$. That is,

$$\sum (E_\eta/E_r)^{1/2} \sim (\eta/r)^{-1/2(D_{1/2})} . \tag{A5}$$

Together, (A4) and (A5) can be written as

$$|\partial u/\partial x|_r \sim K_2 E_r^{1/2} r^{1/2(D^{1/2})} , \tag{A6}$$

where K_2 is another constant. Since we know the r dependence of E_r from Eq. (2) ($E_r \sim r^{\alpha - 1 + d}$, where α is the local singularity strength of ε), we conclude that

$$\alpha_u - 1 + d = (\alpha - 1 + d)/2 + D_{1/2}/2 . \tag{A7}$$

For one-dimensional sections we can write

$$\alpha_u = (\alpha + D_{1/2})/2 . \tag{A8}$$

This means that wherever ε has a singularity of strength α, $|\partial u/\partial x|$ will have a singularity of strength $\alpha_u = (\alpha + D_{1/2})/2$, and that the dimension of the corresponding sets will be

$$f_u(\alpha_u) = f(2\alpha_u - D_{1/2}) . \tag{A9}$$

It should be pointed out that this result can easily be extended to powers other than $\frac{1}{2}$. We can state that the kth power of a multifractal is another multifractal and that their f versus α curves (for one-dimensional sections) are related by

$$\alpha_k = k\alpha - (k-1)D_k . \tag{A10}$$

$$f_k(\alpha_k) = f([\alpha_k + (k-1)D_k]/k) . \tag{A11}$$

It should also be pointed out that if the multifractal spectrum of any given quantity can be modeled in terms of the p model with some p_1 and $p_2 = 1 - p_1$, the kth power of that quantity can be modeled by a nonconservative extension of the model, using instead of p_1 and p_2 the values $p_1' = p_1^k$ and $p_2' = p_2^k$. Now, of course, $p_1' + p_2' \neq 1$, meaning that the total measure changes at each cascade step. When defining the generalized dimensions, one has to normalize by the total measure available at the particular cascade step, and Eq. (11) is easily generalized to

$$D_q' = \log_2[(p_1'^q + p_2'^q)/(p_1' + p_2')^q]/(1-q) . \tag{A12}$$

Using $p_1' = p_1^k$ and $p_2' = p_2^k$ and the usual Legendre transformations to obtain α_k and $f_k(\alpha_k)$, Eqs. (A10) and (A11) are recovered.

APPENDIX B

For experiments on multifractal properties of the velocity derivatives, the turbulent streamwise velocity $u(t)$ was measured in air flow in the wake of a cylinder using hot-wire anemometer. The diameter of the cylinder was 1.7 cm, and the free-stream velocity U was 5 m/s; measurements were made at the centerline of the wake 100 diam downstream of the cylinder. The high-frequency cutoff was about 5 kHz. (This was determined by measuring many spectral densities of the unfiltered velocity signals and noting the frequency at which the energy

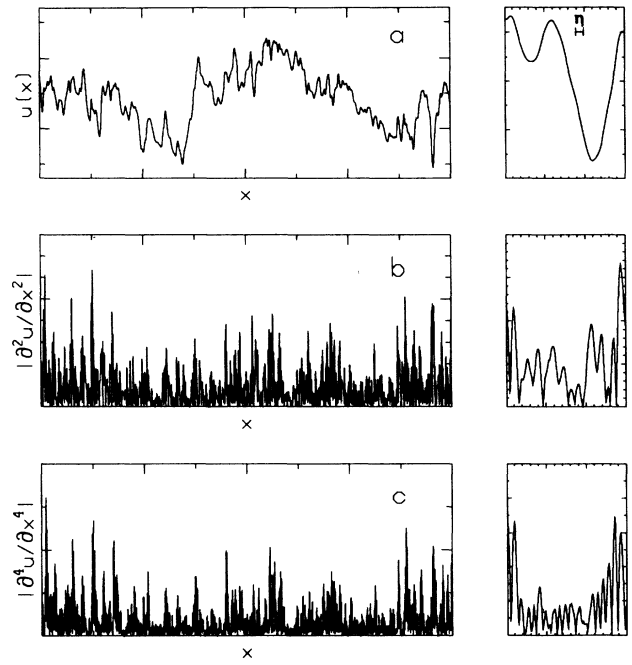

FIG. 11. (a) Velocity signal obtained in the wake of a circular cylinder. In the expanded version, the Kolmogorov microscale η of the flow is indicated. It is seen that the signal is smooth for scales comparable to η. (b) The absolute value of the second-order derivative, and (c) the fourth-order derivative, both obtained (see text) by differentiating the signal (a). The expanded versions to the right correspond to the same expanded region (a).

reaches the noise floor.) It was therefore thought that low-pass filtering the signal at 5kHz was adequate, but the data was acquired at the high rate 20 kHz to ensure a smooth signal for calculating derivatives of high order. The temporal signal $u(t)$ obtained at a single location was then interpreted as a streamwise spatial cut $u(x)$ through the flowfield at a single instant, using Taylor's frozen-flow hypothesis. An experimental substantiation of this hypothesis in a similar context has been given by Prasad *et al.*[18] The signal was digitized using a 12-bit analog-to-digital converter on a Masscomp 5500 computer.

In order to smooth out the digitizer noise when obtaining the derivatives $\partial^n u/\partial x^n$ for each point x_i of the signal, a fourth-order polynomial was fitted locally to the data:

$$P_i(x)=\sum_{k=0}^{4} a_{ik}(x-x_i)^k \sim u(x) , \tag{B1}$$

where the a_{ik} were obtained by minimizing the least-square error using 25 points $u(x_{i-12})$ through $u(x_{i+12})$ around x_i. The derivatives were then evaluated from (B1) at $x=x_i$ according to

$$\partial^n u/\partial x^n|_i = n!\, a_{in} . \tag{B2}$$

This procedure was repeated for every point of the signal. Figure 11(a) shows a typical velocity signal $u(x)$. Also shown is an enlargement of the signal, where the Kolmogorov length scale is indicated. It is clear that the data-acquisition frequency is sufficiently high to produce a smooth signal. Figures 11(b) and 11(c) show $|\partial^2 u/\partial x^2|$ and $|\partial^4 u/\partial x^4|$, as well as the expanded regions corresponding to that shown in detail in Fig. 11(a). As n goes up, stronger, and presumably less space filling, peaks are visible. Also, the signal corresponding to the fourth derivative of u is still smooth when viewed at scales smaller than η but, as expected, more activity is seen at these scales.

In order to obtain the f versus α curves of $|\partial^n u/\partial x^n|$, we processed these signals as described in detail in Ref. 9 for the dissipation signals. First, we obtain the generalized dimensions D_q; scaling of over 1.5 decades was observed, thus justifying the treatment of the absolute value of the derivatives as multifractal measures. Sixteen different signals, each 50 L long, were used. The resulting D_q curves were averaged. The variability of D_q was ± 0.035 at $q=8$, ± 0.002 at $q=2$, and ± 0.055 at $q=-8$. The f versus α curves were then computed using the averaged D_q curves for $n=1-4$.

[1]J. Leray, Acta Math. Acad. Sci. Hung. **63**, 193 (1934).
[2]B. B. Mandelbrot, C. R. Acad. Sci. **282A**, 119 (1976).
[3]V. Scheffer, C. R. Acad. Sci. **282A**, 121 (1976); Commun. Math. Phys. **55**, 97 (1977); **61**, 41 (1978); **73**, 1 (1980).
[4]L. Caffarelli, R. Kohn, and L. Nirenberg, Commun. Pure Appl. Math. **35**, 771 (1982).
[5]A. J. Chorin, Commun. Math. Phys. **83**, 517 (1982).
[6]U. Frisch and R. Morf, Phys. Rev. A **23**, 2673 (1981).
[7]E. D. Siggia and A. Pumir, Phys. Rev. A. **55**, 1749 (1985).
[8]B. B. Mandelbrot, *The Fractal Geometry of Nature* (Freeman, San Fransisco, 1982).
[9]C. Meneveau and K. R. Sreenivasan, in *The Physics of Chaos and Systems Far from Equilibrium*, edited by Minh-Duong Van (North-Holland, Amsterdam, 1987), p. 49.
[10]It appears reasonable to expect that the various components of energy dissipation must have the same multifractal spectrum as that of the sum. This has been shown to be true in Ref. 18 for scalar dissipation. Equivalently, the various power-law dependences on the Reynolds number must be identical for all components, the possible differences confined entirely to the preexponential factors. A further plausibility argument in support of this conclusion is that, if it were otherwise, some one component of the energy dissipation would overwhelm all others, and lead to the unlikely prospect of increasing anisotropy of the small scales with increasing Reynolds number.
[11]U. Frisch and G. Parisi, in *Turbulence and Predictability in Geophysical Fluid Dynamics and Climate Dynamics*, edited by M. Ghil, R. Benzi, and G. Parisi (North-Holland, New York, 1985), p. 84.
[12]T. C. Halsey, M. H. Jensen, L. P. Kadanoff, I. Procaccia, and B. I. Shraiman, Phys. Rev. A **33**, 1141 (1986).
[13]B. B. Mandelbrot, J. Fluid Mech. 62, 331 (1975).
[14]H. G. E. Hentschel and I. Procaccia, Physica D **8**, 435 (1983).

[15]L. F. Richardson, *Weather Prediction by Numerical Procedure* (Cambridge University Press, Cambridge, 1922).
[16]A. N. Kolmogorov, C. R. Acad. Sci. USSR 30, 299 (1941).
[17]K. R. Sreenivasan, R. R. Prasad, C. Meneveau, and R. Ramshankar, *Fractals in Geophysics,* special edition, edited by B. B. Mandelbrot and C. Scholz (PAGEOPH Verlag, Birkhauser, in press).
[18]R. R. Prasad, C. Meneveau, and K. R. Sreenivasan, Phys. Rev. Lett. **61**, 74 (1988).
[19]G. K. Batchelor, *The Theory of Homogeneous Turbulence* (Cambridge University Press, Cambridge, 1953).
[20]C. E. Shannon and W. Weaver, *The Mathematical Theory of Communications* (University of Illinois Press, Chicago, 1949).
[21]M. Feigenbaum, M. H. Jensen, and I. Procaccia, Phys. Rev. Lett. 57, 1507 (1986).
[22]A. Chhabra, R. V. Jensen and K. R. Sreenivasan (unpublished).
[23]U. Frisch, P. L. Sulem, and M. Nelkin, J. Fluid Mech. **87**, 719 (1978).
[24]C. Meneveau and K. R. Sreenivasan, Phys. Rev. Lett. **59**, 1424 (1987).
[25]A. Y.-S. Kuo and S. Corrsin, J. Fluid Mech. **56**, 447 (1972).
[26]Wm. T. Ashurst, A. R. Kerstein, R. M. Kerr, and C. H. Gibson, Phys. Fluids **30**, 2343 (1987).
[27]H. Mori, Suppl. Prog. Theor, Phys. **69**, 111 (1980).
[28]H. G. E. Hentscel and I. Procaccia, Phys. Rev. Lett. **49**, 1158 (1982).
[29]A. Chorin, Phys. Rev. Lett. **60**, 1947 (1988).